Supporting Information for

Fully automated, label-free isolation of extracellular vesicles from whole blood for cancer diagnosis and monitoring

Vijaya Sunkara[†, §, ‡], Chi-Ju Kim[†, §, ‡], Juhee Park[§], Hyun-Kyung Woo[†, §], Dongyoung Kim[§], Hong Koo Ha[‖], Mi-Hyun Kim[⊥], Youlim Son[#], Jae-Ryong Kim[#], Yoon-Kyoung Cho[†, §, *]

[†]Department of Biomedical Engineering, School of Life Sciences, Ulsan National Institute of Science and Technology (UNIST), Ulsan 44919, Republic of Korea;
[§]Center for Soft and Living Matter, Institute for Basic Science (IBS), Ulsan 44919, Republic of Korea;
[‖]Department of Urology, Pusan National University Hospital, Pusan National University School of Medicine, Busan 49241, Republic of Korea;
[⊥]Department of Internal Medicine, Pusan National University Hospital, 179, Gudeok-ro, Seo-Gu, Busan 49241, Republic of Korea;
[#] Department of Biochemistry and Molecular Biology, Smart-aging Convergence Research Center, College of Medicine, Yeungnam University, Daegu 42415, Republic of Korea.

[‡] These authors contributed equally to this work.

*Corresponding author: E-mail: ykcho@unist.ac.kr

Keywords: extracellular vesicles, liquid biopsy, lab-on-a-disc, size-based filtration, ELISA

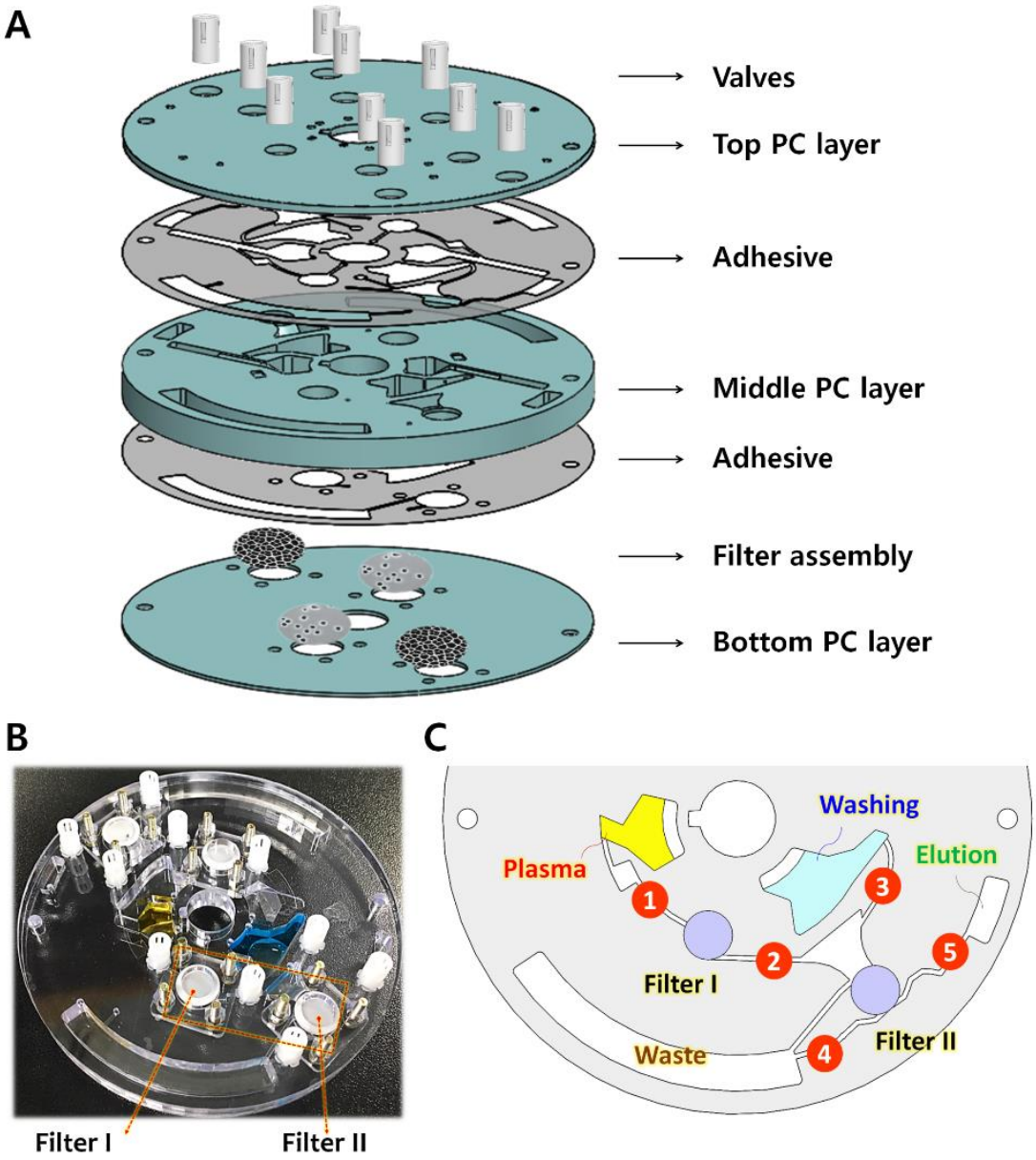

Figure S1. (**A**) Expanded view of disc depicting top, middle, and bottom layers of polycarbonate (PC) with two layers of double-sided adhesive tapes and filters. (**B**) Photograph and (**C**) schematic showing microfluidic layout of Exodisc-P to enrich EVs starting from plasma, which is identical to Exodisc-B, except for the blood separation chamber.

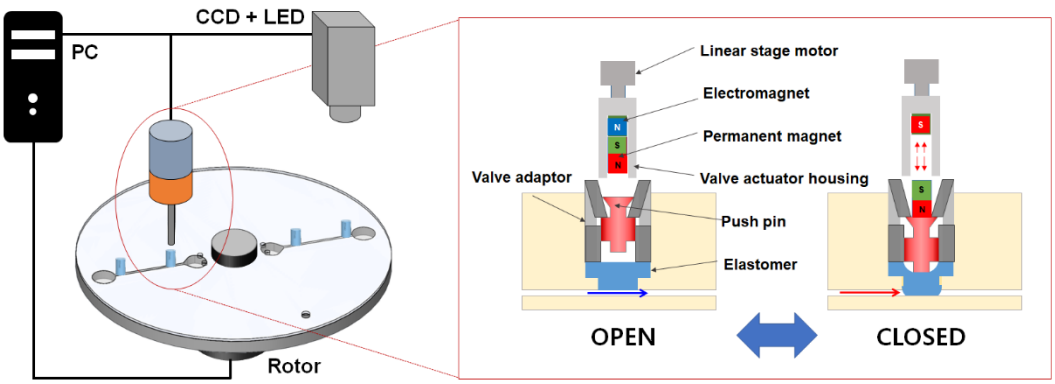

Figure S2. Schematic illustration depicting operation of individually addressable diaphragm valves (ID valves). Side view of the fluidic channel shows the ID valve in open and closed states; the valve can be reversibly actuated by manipulating electromagnet polarity. For valve actuation, spinning disc was stop-aligned and spun again for liquid transfer.

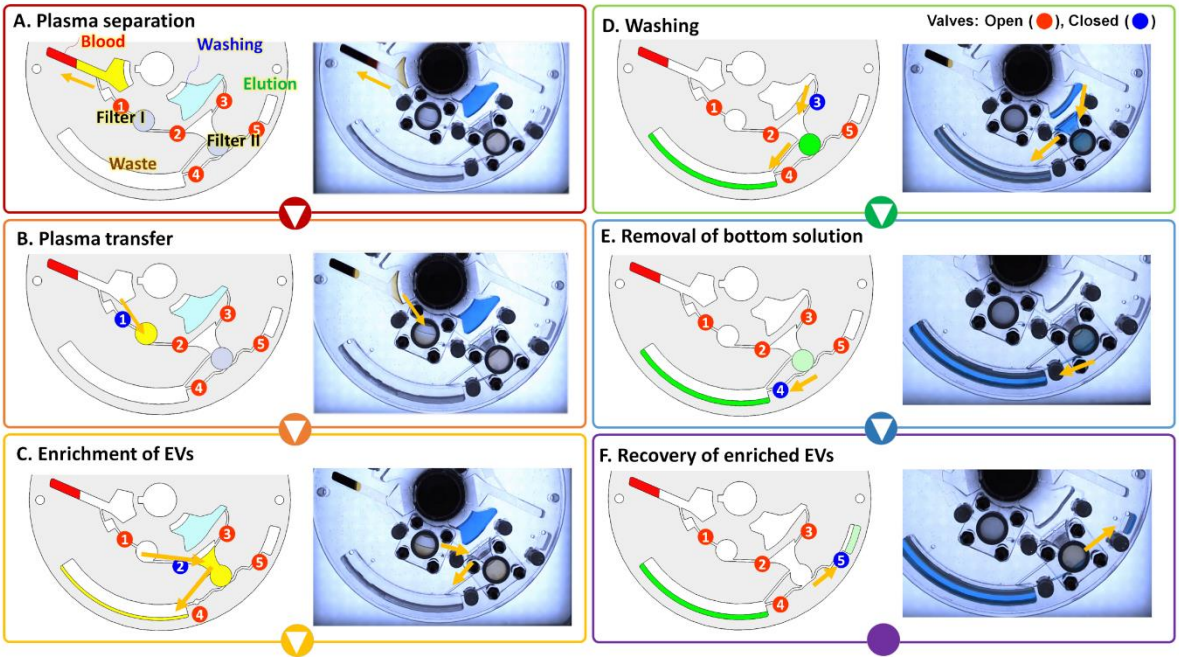

Figure S3. Schematics (left) and CCD images (right) of overall process of EV-enrichment from whole-blood samples on a spinning disc—(**A**) Plasma separation from whole blood; (**B**) transfer of plasma to filtration chamber by opening valve #1; (**C**) EV enrichment on filter II by opening valve #2; (**D**) washing of enriched EV by opening valve #3; (**E**) removal of solution under filter II by opening valve #4; (**F**) transfer of enriched EV to collection chamber for recovery by opening valve #5.

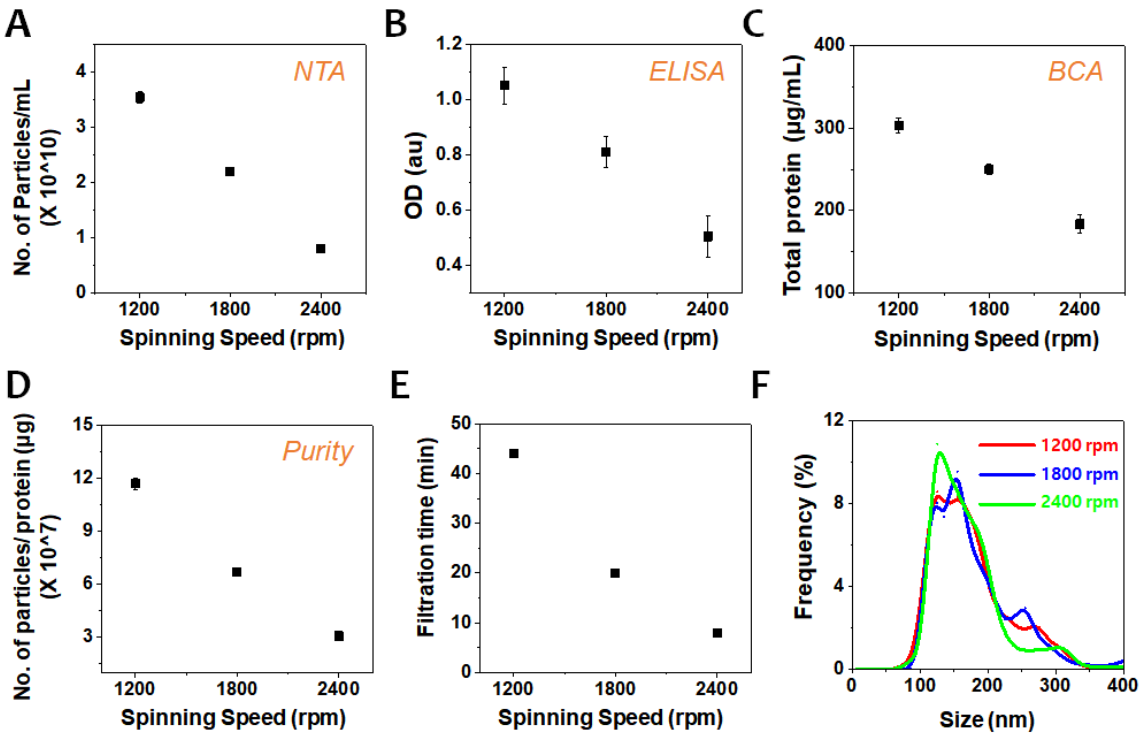

Figure S4. Effect of spinning speed on the performance of EV enrichment using D100. (**A**) Number of EVs, (**B**) CD9-CD81 sandwich ELISA results, (**C**) total protein quantification based on BCA measurements, (**D**) purity measured by number of particles per total protein content, (**E**) filtration time, and (**F**) the size-distribution profiles of EVs isolated are characterized at different spinning speed. The mean values were plotted with the standard deviation represented by error bars.

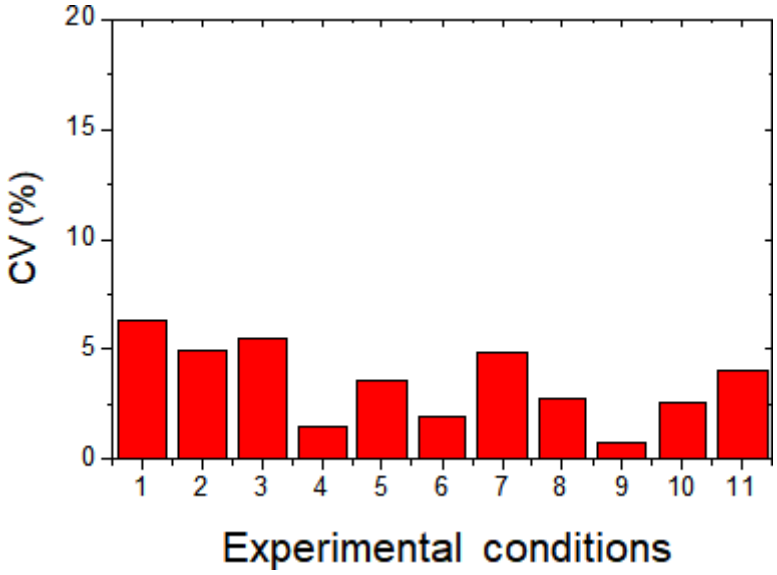

Figure S5. The coefficient of variation (CV %) of CD9-CD81 ELISA signal obtained from 11 different experimental conditions were calculated to measure the reproducibility of D100. At each experimental condition, at least three repeats using three individual units using one and half disc were tested. The average CV% from the hand-made prototype device was less than 7%, which can be further improved by using injection-molded device.

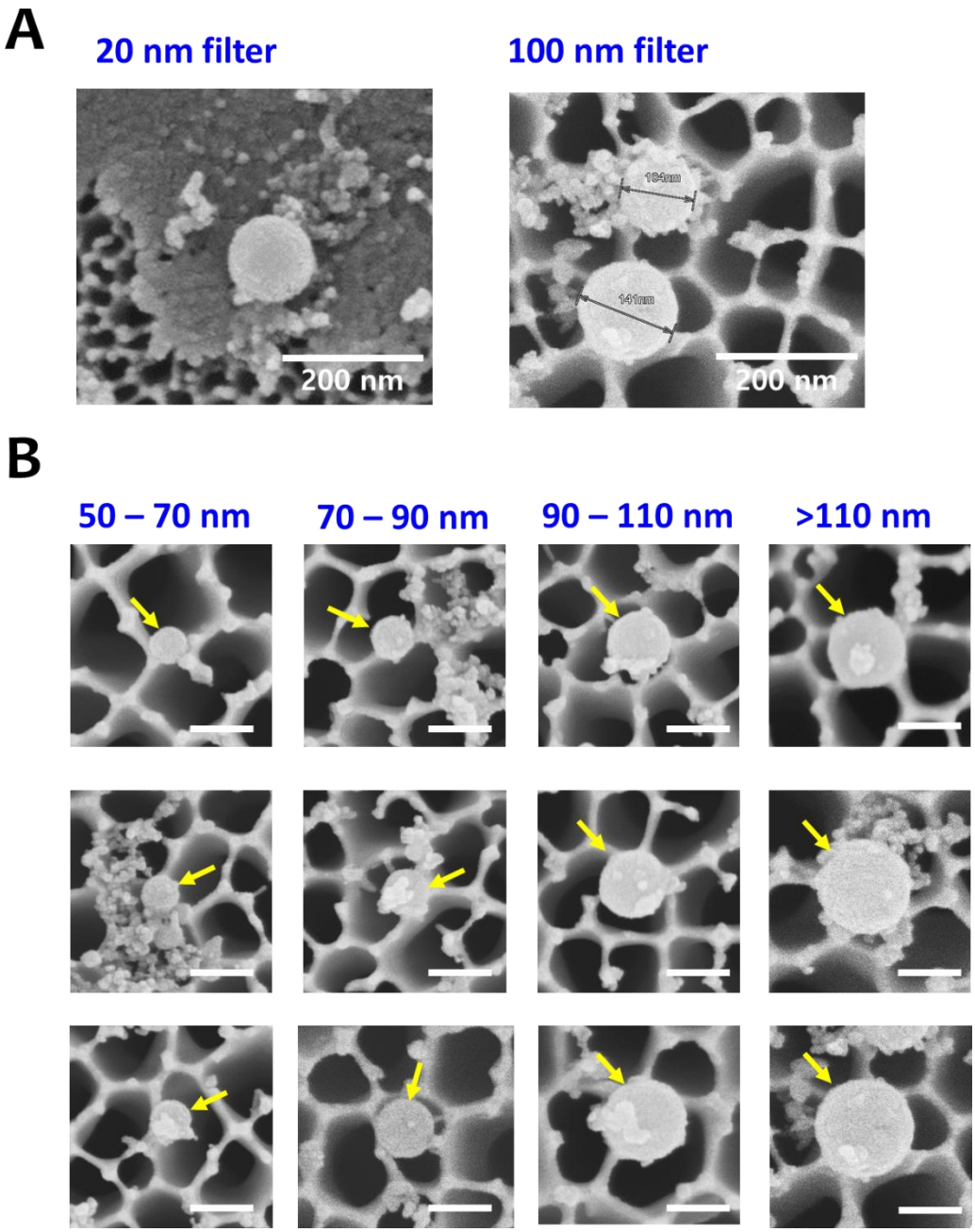

Figure S6. (**A**) Representative SEM images of 20 nm and 100 nm filters after plasma filtration on D20 and D100, respectively. (**B**) Representative SEM images of EVs of different size ranges between 50 and 200 nm isolated using D100.

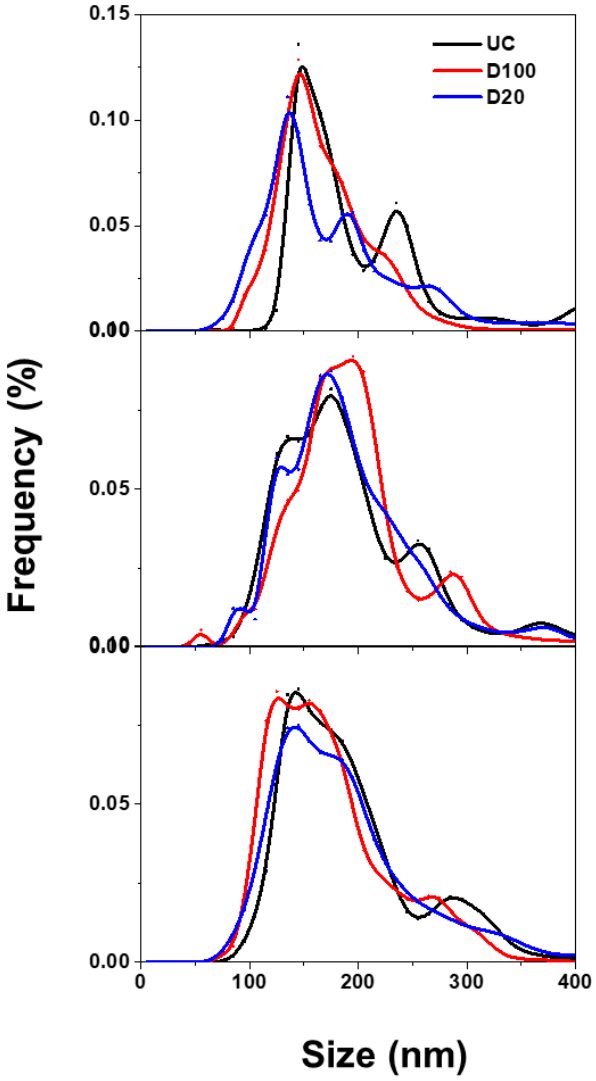

Figure S7. Size distribution profiles of EVs isolated from different samples via UC, D20, and D100.

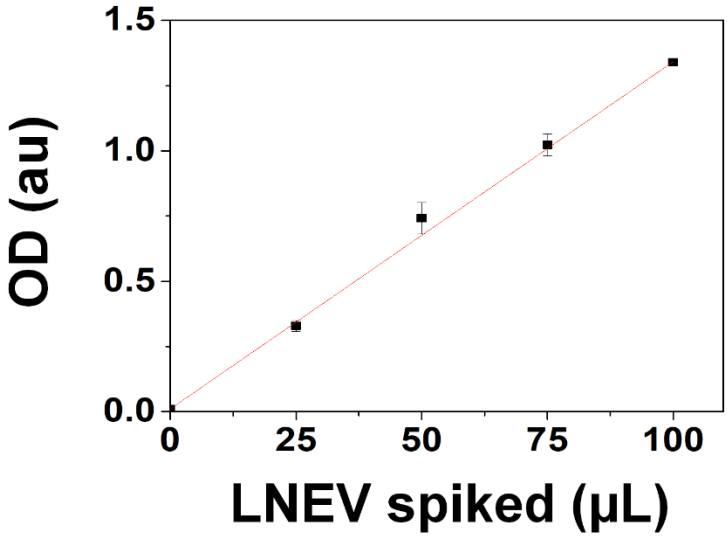

Figure S8. CD9-CD81 sandwich ELISA results from LNCaP-cell-derived EVs spiked in the plasma sample. At each experimental condition, the plasma volume and the total sample volume was fixed at 100 µL and 200 µL, respectively. The remaining volume was adjusted by adding PBS. All measurements were performed thrice. The mean values were plotted with the standard deviations represented by error bars.

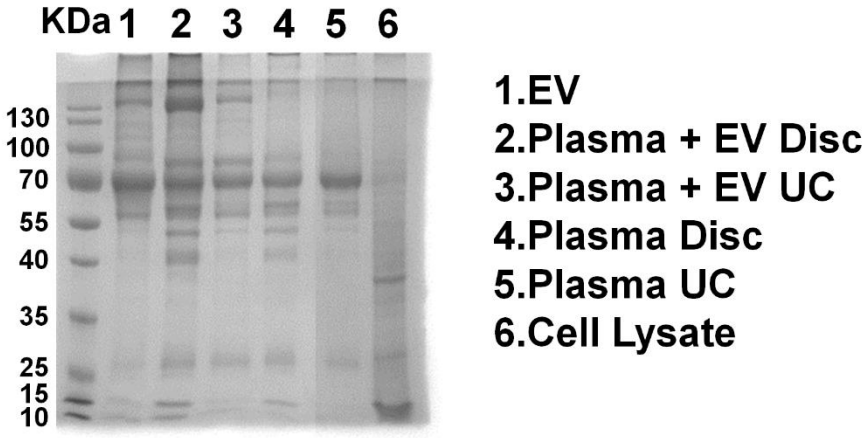

Figure S9. Gel electrophoresis analysis of protein content of EV lysates; images were assessed by Coomassie blue staining of 1. LNEV; 2. LNEV-spiked-plasma with EV isolated using Exodisc-P; 3. LNEV-spiked-plasma with EV isolated by UC; 4. plasma EV obtained on Exodisc-P; 5. plasma EV prepared by UC; and 6. cell lysates.

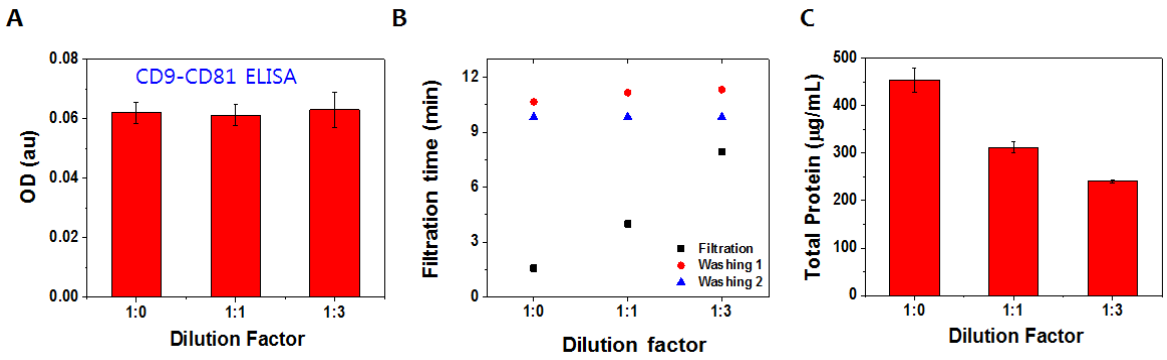

Figure S10. Effect of plasma dilution factor on (**A**) capture yield, (**B**) filtration time, and (**C**) total protein amount. The plasma sample (100 µL) from a cancer patient was diluted with PBS buffer with dilution factors of 1:1 and 1:3, resulting in total volumes of 200 µL and 400 µL. When the diluted plasma sample was used, i.e., total sample volume was increased with the same plasma loading volume, the capture efficiency remained the same (A) while the filtration time increased (B) and the total protein content decreased (C). The bars/markers and the error bars represent the mean ± s.e.m.

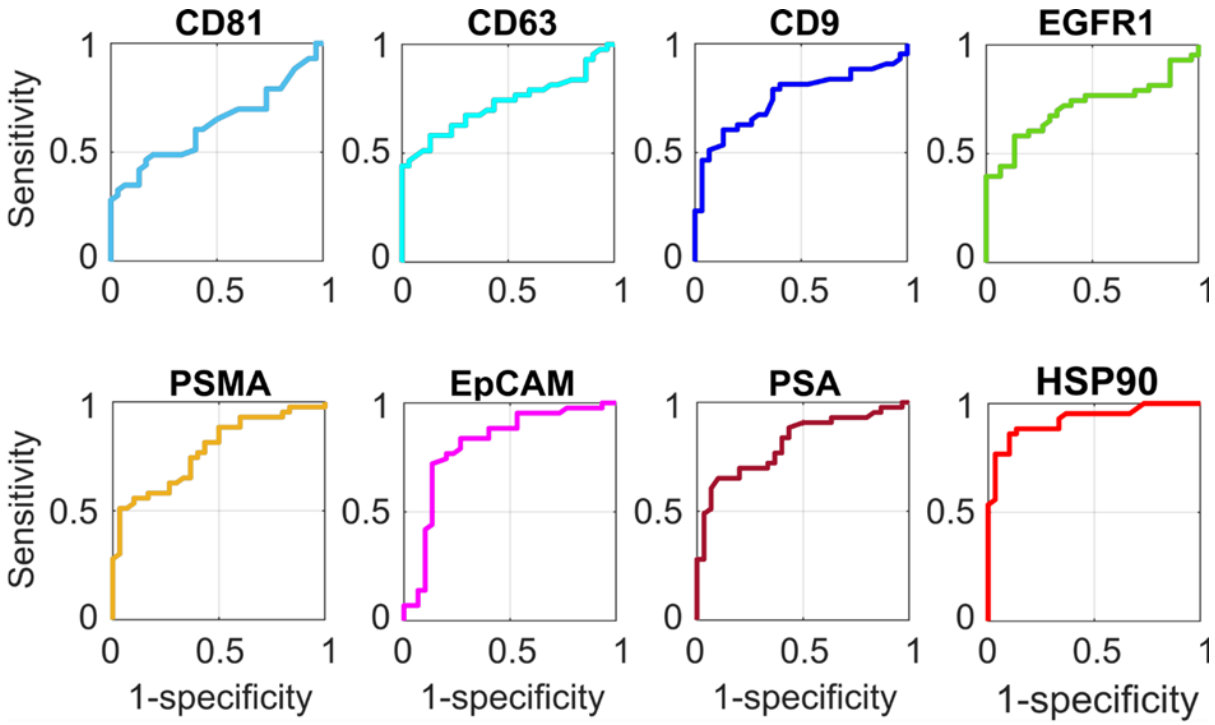

	CD81	CD63	CD9	EGFR1	PSMA	EpCAM	PSA	HSP90
AUC	0.629	0.728	0.750	0.714	0.777	0.806	0.812	0.924
SE	0.071	0.066	0.064	0.068	0.057	0.054	0.054	0.033
Accuracy	0.616	0.685	0.712	0.699	0.699	0.781	0.740	0.877
Sensitivity	0.488	0.628	0.605	0.581	0.744	0.767	0.698	0.860
Specificity	0.800	0.767	0.867	0.867	0.633	0.800	0.800	0.900
Cut-off	0.048	0.089	0.036	0.107	0.242	0.056	0.066	0.087

Figure S11. ROC analysis of human-plasma-driven EV-protein expressions following ROC and cutoff criteria evaluated for each marker: area under ROC curve (AUC), standard error (SE), accuracy, sensitivity, specificity, cutoff (OD). The optimum cut-off value was calculated to maximize the sensitivity and specificity values, which is co-located in the nearest point to (0,1) in the ROC curve. This was carried out by finding the minimum of the distance d to the top-left corner of the ROC curve, $d = \sqrt{(1 - sensitivity)^2 + (1 - specificity)^2}$. HSP90 ranks first with regard to all evaluation criteria.

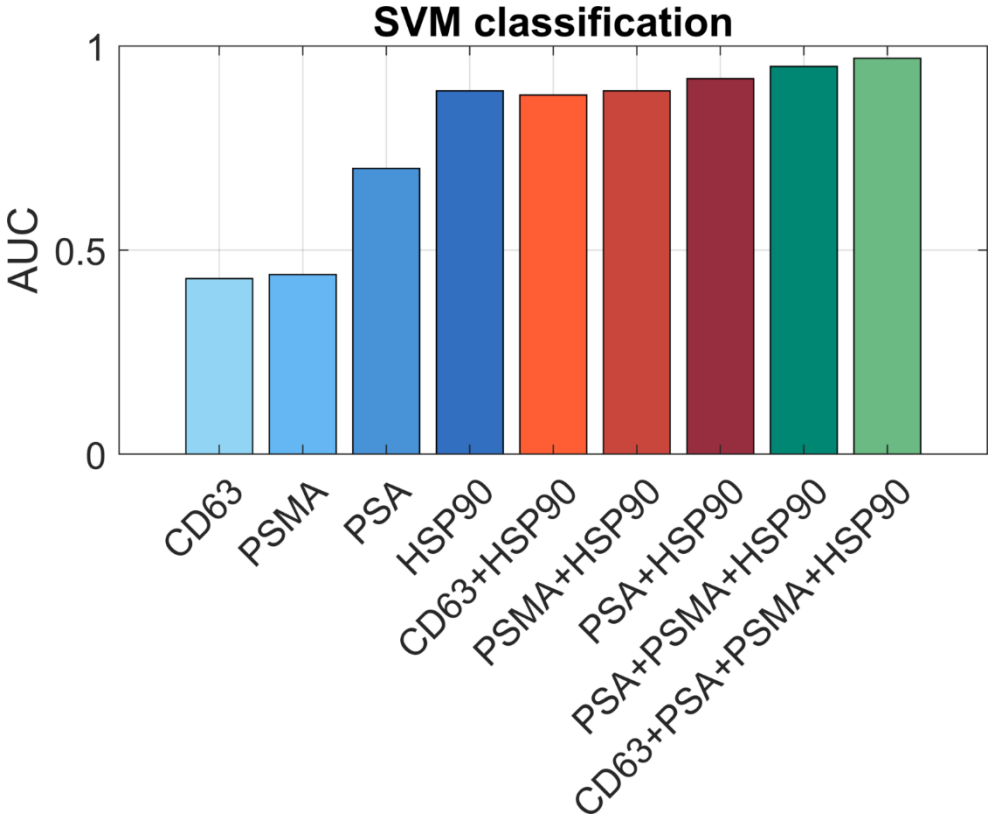

Figure S12. Prostate cancer patient classification by SVM analysis. SVM classifiers were created from ELISA results of CD63, PSMA, PSA, and/or HSP90 and their area under the curve (AUC) were evaluated from the ROC analysis.

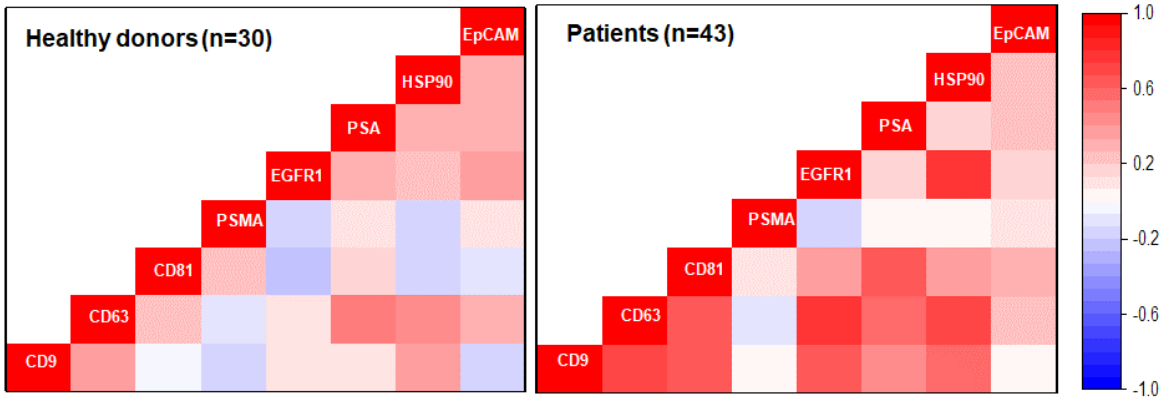

Pca samples (n=43)		
Positive correlations		
Markers	**r (Spearman)**	**Significance**
CD9-CD63	**0.72**	**5.8E-8**
CD9-CD81	**0.60**	**1.8E-5**
CD81-CD63	**0.64**	**3.2E-6**
CD9-EGFR	**0.64**	**4.2E-6**
CD9-HSp90	**0.53**	**2.2E-4**
CD63-EGFR	**0.76**	**2.6E-9**
CD63-PSA	**0.59**	**3.6E-5**
CD63-HSP90	**0.68**	**4.1E-7**
CD81-PSA	**0.65**	**2.8E-6**
EGFR-HSP90	**0.80**	**1.7E-10**
HD (n=30)		
CD63-PSA	**0.50**	**0.005**
All others	**< 0.50**	

Figure S13. Heat map of Spearman correlation for tested markers CD9, CD63, CD81, PSMA, EGFR1, PSA, HSP90, and EpCAM and expression levels measured via ELISA. The table presents a list of positive correlations in 43 prostate-cancer patients and 30 healthy donors.

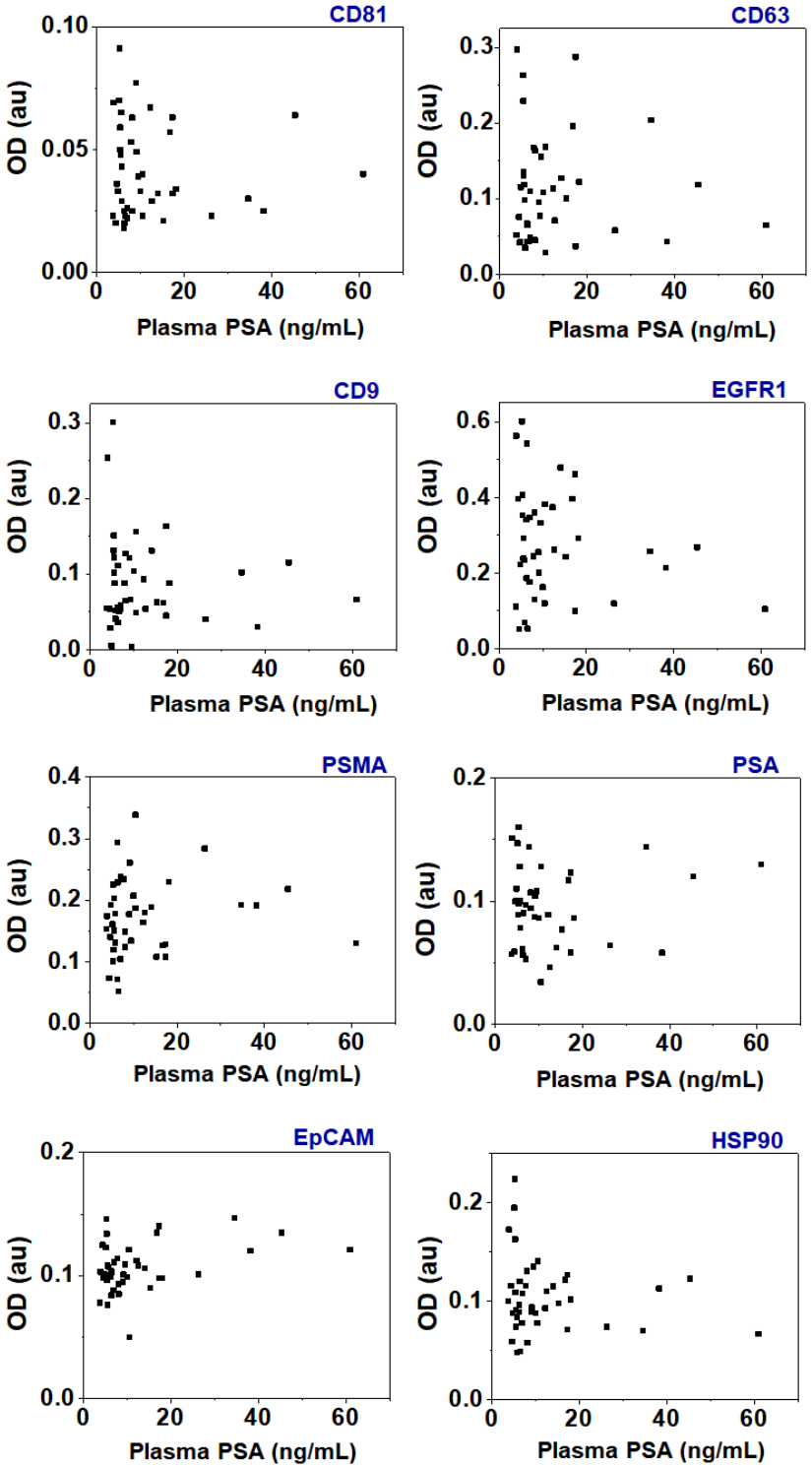

Figure S14. Correlation between EV-marker expression and plasma PSA concentration in prostate-cancer patients.

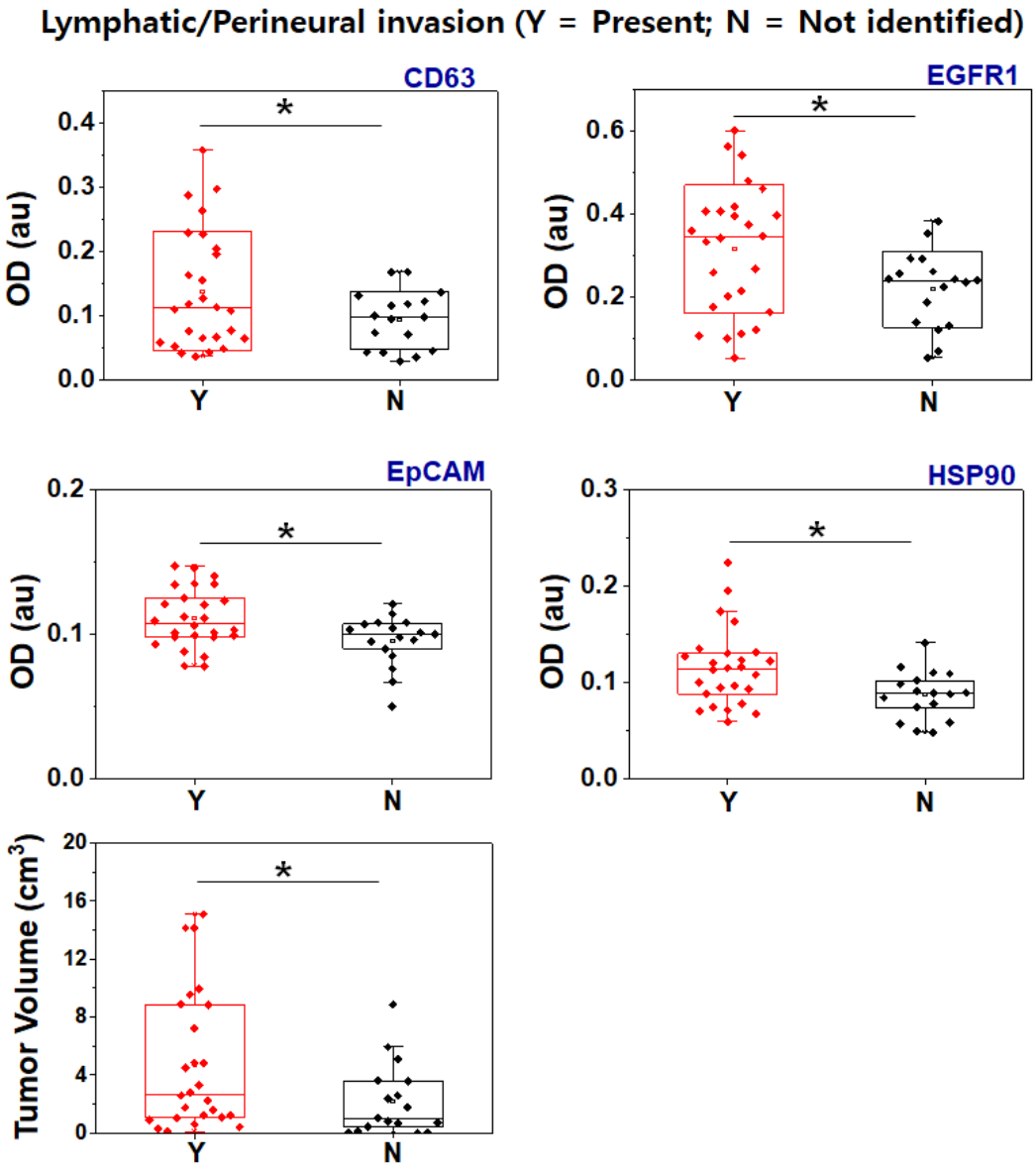

Figure S15. Results concerning CD63, EGFR1, EpCAM, and HSP90 levels along with tumor volume in prostate-cancer patients. Significantly higher values were noted in samples with lymphatic and/or perineural invasion (Y, n = 26) compared to those without the said invasion (N, n = 17). The box plot indicates the 75th percentile (top line of the box), median (middle line of the box), 25th percentile (bottom line of the box), and 5th and 95th percentiles (whiskers) with raw measurements in scattered dots.

Table S1. Detailed disc operation program for EV isolation from whole blood.

No.	Step	Spin speed (rpm)	Duration	Operation
1	Plasma separation	3600	5 min	Plasma separation from whole blood (600 μL)
2	Plasma transfer	2400	20 s	Open valve **#1** to transfer plasma sample (200 μL) to pre-filtration chamber integrated with TEPC membrane having pore diameter of 600 nm
3	EV filtration	1200	10 min	Open valve **#2** to filtrate EV sample from pre-filtered plasma through AAO membrane having pore diameter of 100 nm
4	Wash	1200	20 min	Open valve **#3** to wash EV sample on 100-nm filter
5	Bottom-solution removal	1800	10 s	Open valve **#4** to remove solution under 100-nm AAO membrane
6	EV retrieval	1800	10 s	Open valve **#5** to retrieve EV sample
	Total time		**< 36 min**	

EV = extracellular vesicle; TEPC = track-etched polycarbonate; AAO = anodic aluminum oxide.

Table S2. mRNA Expression level of EV samples prepared by Exodisc and UC

Gene	C_T		$-\Delta C_T = (C_T)\_UC - (C_T)\_Exodisc$	*Fold change compared to UC* 2^-ΔCT
	UC	Exodisc-P		
GAPDH	29.29 ± 0.08	24.79 ± 0.70	4.50 ± 0.13	22.6 ± 1.0 X
CD63	34.09 ± 0.74	28.95 ± 0.13	5.14 ± 0.11	35.4 ± 1.1 X
CD81	38.04 ± 0.23	32.61 ± 0.10	5.43 ± 0.04	43.1 ± 1.0 X
Average:			**5.02 ± 0.18**	**33.7 ± 1.0 X**

The Ct values of three genes, GAPDH, CD63, and CD81 were measured from EV samples prepared by UC and Exodisc. In this study, the absolute amount of EVs prepared by the different methods were the main interests and therefore we compared mRNA expression level of EVs prepared by Exodisc with the sample prepared by the gold standard method, UC. Therefore ΔCT was defined as Avg. C_T_Exodisc-P – Avg. C_T_UC. To calculate the fold change compared to the UC method, 2^-ΔCT was calculated. The standard deviation of the fold change was calculated by using the coefficient of variation (CV), defined as the square root of (CV_UC^2+ CV_Exodisc-P^2), multiplied by the mean of ΔC_T.

Table S3. Summary of prostate-cancer-patient information.

	Patient
Total case	43
Age (years)	
Median	73
Range	63–83
Serum PSA levels (ng/ml)	
< 4	2
> 4	39
Unknown	2
Stage	
I	0
II	29
III	12
IV	0
Unknown	2
Gleason Score	
≤ 7	30
> 8	11
unknown	2
Lymphatic invasion	
present	3
Not identified	39
unknown	1
Perineural invasion	
Yes	15
No	27
Unknown	1

Table S4. List of antibodies used in this study.

Type	*Antibody*	*Company*	*Catalogue Number*	*Species*
Primary antibodies	Anti-CD9 antibody [MEM-61]	Abcam	ab2215	Mouse monoclonal
	Anti-PSMA antibody [YPSMA-1]	Abcam	ab19071	Mouse monoclonal
	Anti-HSP90 antibody [16F1]	Abcam	ab13494	Rat monoclonal
	Anti-EpCAM antibody [MOC-31]	Abcam	ab187270	Mouse monoclonal
	Anti-PSA antibody	SD		Mouse monoclonal
	Human CD63 Purified H5C6	BD	BD556019	Mouse monoclonal
	Human CD81 Purified JS-81	BD	BD555675	Mouse monoclonal
	Human CD9 Purified M-L13	BD	BD555370	Mouse monoclonal
	Purified Mouse Anti-HSP90	BD	BD610418	Mouse monoclonal
Secondary/ Detection antibodies	Anti-CD81 antibody	LS	LS-C134650	Mouse Monoclonal [clone 1.3.3.22]
	Anti-EGFR1 antibody [EFGR-1]	Abcam	ab24293	Mouse monoclonal
	Human PSMA/FOLH1/NAALADase I	R&D	BAF4234	Polyclonal Sheep IgG
	Goat Anti-Rabbit IgG H&L (HRP)	Abcam	ab6721	rabbit polyclonal IgG
	Streptavidin-HRP	R&D	DY998	
ELISA kit/Duo set	Human Serum Albumin DuoSet ELISA	R&D	DY1455	
	Human Kallikrein 3/PSA immunoassay	R&D	DKK300	

SD company (SD), BD Biosciences (BD), LS Bioscience (LS), R&D Systems (R&D)

Table S5. List of primer sequences used in RT-PCR analysis.

GAPDH	Forward	5’-ATGGGTGTGAACCATGAGAA-3’
	Probe	5’-CCTCAAGATCATCAGCAATGCCTCC-3’
	Reverse	5’-GTGCTAAGCAGTTGGTGGTG-3’
CD9	Forward	5’-GGCTTCCTCTTGGTGATATTCG-3’
	Probe	5’-TCCTGGACTTCCTTAATCACCTCATCCT-3’
	Reverse	5’-GGCTCATCCTTGGTTTTCAG-3’
CD63	Forward	5′-AACGAGAAGGCGATCCATAAG-3′
	Probe	5′-CCTCGACAAAAGCAATTCCAAGGGC-3′
	Reverse	5′-GCAGGCAAAGACAATTCCC-3′
CD81	Forward	5’-AGATCGCCAAGGATGTGAAG-3’
	Probe	5’-AGCAGTCAAGCGTCTCGTGGAAG-3’
	Reverse	5’-AGGTGGTCAAAGCAGTCAG-3’

Movie S1: Visualization of EV isolation from whole blood sample using Exodisc-B.